References

ALTOMARE, A., BURLA, M. C., CASCARANO, G., GIACOVAZZO, C. & GUAGLIARDI, A. (1993). *Acta Cryst.* A**49**, 342–346.

ALTOMARE, A., CASCARANO, G., GIACOVAZZO, C. & GUAGLIARDI, A. (1993). *J. Appl. Cryst.* **26**, 343–350.

BABUDRI, F., FLORIO, S., ZUCCARO, L., CASCARANO, G. & STASI, F. (1985). *Tetrahedron*, **41**, 569–573.

BROMLEY, L., COLLINGWOOD, S., DAVIES, S. G., OTHEN, E. J. & WATKIN, D. J. (1990). Private communication.

BURLA, M. C., CAMALLI, M., CASCARANO, G., GIACOVAZZO, C., POLIDORI, G., SPAGNA, R. & VITERBO, D. (1989). *J. Appl. Cryst.* **22**, 389–393.

BURLA, M. C., CASCARANO, G. & GIACOVAZZO, C. (1992). *Acta Cryst.* A**48**, 906–912.

BURLA, M. C., CASCARANO, G., GIACOVAZZO, C., NUNZI, A. & POLIDORI, G. (1987). *Acta Cryst.* A**43**, 370–374.

CASCARANO, G., DOUGGY-SMIRI, L. & NGUYEN-HUY DUNG (1987). *Acta Cryst.* C**43**, 2050–2053.

CASCARANO, G., GIACOVAZZO, C., BURLA, M. C., NUNZI, A. & POLIDORI, G. (1984). *Acta Cryst.* A**40**, 389–394.

CASCARANO, G., GIACOVAZZO, C., CAMALLI, M., SPAGNA, R., BURLA, M. C., NUNZI, A. & POLIDORI, G. (1984). *Acta Cryst.* A**34**, 278–283.

CASCARANO, G., GIACOVAZZO, C. & GUAGLIARDI, A. (1992). *Acta Cryst.* A**48**, 859–865.

CASCARANO, G., GIACOVAZZO, C. & VITERBO, D. (1987). *Acta Cryst.* A**43**, 22–29.

CERRINI, S., LAMBA, D., BURLA, M. C., POLIDORI, P. & NUNZI, A. (1988). *Acta Cryst.* C**44**, 489–495.

COCHRAN, W. (1952). *Acta Cryst.* **5**, 65–67.

DECLERCQ, J. P., GERMAIN, G. & WOOLFSON, M. M. (1979). *Acta Cryst.* A**35**, 622–626.

GIACOVAZZO, C., BURLA, M. C. & CASCARANO, G. (1992). *Acta Cryst.* A**48**, 901–906.

HULL, S. & IRWIN, M. J. (1978). *Acta Cryst.* A**34**, 863–870.

KARLE, I. L. & KARLE, J. (1966). *Acta Cryst.* **21**, 849–859.

KARLE, J. & HAUPTMAN, H. (1956). *Acta Cryst.* **9**, 635–651.

KOJIĆ-PRODIĆ, B., RUŽIĆ-TOROŠ, Z., BRESCIANI-PAHOR, N. & RANDACCIO, L. (1980). *Acta Cryst.* B**36**, 1223–1225.

MAIN, P. (1977). *Acta Cryst.* A**33**, 750–757.

NGUYEN-HUY DUNG, VO-VAN TIEN, BEHM, H. J. & BEURSKENS, P. T. (1987). *Acta Cryst.* C**43**, 2258–2260.

SCORDARI, F. & STASI, F. (1990). *Z. Kristallogr.* **190**, 47–62.

SHELDRICK, G. M. (1991). In *Direct Methods in Solving Crystal Structures*, edited by H. SCHENK. New York: Plenum.

Acta Cryst. (1994). A**50**, 27–32

Dynamical Treatment of the Splitting of Higher-Order-Laue-Zone Lines Induced by Dislocations in an Icosahedral Quasicrystal*

BY JIANGLIN FENG, HUAMIN ZOU, RENHUI WANG, YANFA YAN AND MINGXING DAI

Department of Physics, Wuhan University, 430072 *Wuhan, People's Republic of China*

(*Received* 13 *August* 1991; *accepted* 7 *May* 1993)

Abstract

The dynamical theory of electron diffraction for quasicrystals (QCs) was used to treat the splitting behaviour of higher-order-Laue-zone (HOLZ) lines induced by dislocations in icosahedral quasicrystals (IQCs). The influences of some parameters on the splitting of HOLZ lines were calculated. On the basis of this calculation, several experimental convergent-beam electron diffraction patterns from the aluminium–copper–iron IQC were simulated. Good agreement between the experiment and the simulation confirms the correctness of the dynamical theory of electron diffraction for QCs.

1. Introduction

For crystals, the dynamical theory of electron diffraction (Hirsch, Howie, Nicholson, Pashley & Whelan, 1965) has been successfully used to explain almost all the experimental phenomena. Head, Humble, Clarebrogh, Mortoon & Forwood (1973) developed a matching program to identify defects such as dislocations and stacking faults by use of the two-beam approximation of the dynamical theory. Tanaka, Terauchi & Kanemaya (1988) discussed the defocus convergent-beam electron diffraction (CBED) patterns from defected crystals and determined the Burgers vectors of the dislocations and the displacement vectors of the faults. Lu, Wen, Zhang & Wang (1990), Zou, Yao & Wang (1991) and Kuo & Wang (1992) developed the many-beam method to simulate experimental CBED patterns and obtained good agreement. Dynamical calculation or simulation has become a powerful tool to analyse and study defects in crystals.

In this paper, we propose a method for treatment of the splitting of the higher-order-Laue-zone (HOLZ) lines in icosahedral quasicrystals (IQCs). This treatment is based on the dynamical theory of electron diffraction for QCs (see §2) proposed by

* Project supported by the National Natural Science Foundation of China.

Wang & Cheng (1987) and Cheng & Wang (1989). By using this dynamical theory, Wang, Wang & Deng (1991) successfully analysed small dislocation loops in the aluminium–silicon–manganese (Al–Si–Mn) IQC. Moreover, Wang & Dai (1993) determined the six-dimensional indices of the Burgers vector of dislocations in the (aluminium–copper–iron) (Al–Cu–Fe) IQC to be equal to $1/2[0,-1,1,0,-1,1]$, also using this dynamical theory. These facts encourage us to apply this dynamical theory of electron diffraction for QCs to the simulation of the CBED patterns from QCs. To aid in the choice of appropriate parameters in the simulation, in the present work we studied the influences of several parameters on the splitting behaviour of HOLZ lines (§3). We then successfully simulated some experimental CBED patterns (§4).

2. Theory

The computer program was established on the basis of the wave-mechanical formulation of many-beam dynamical theory developed by Jones, Rackham & Steeds (1977) using the scattering-matrix method (Hirsch *et al.*, 1965). The theory was formed originally for crystals and extended by Wang & Cheng (1987) and Cheng & Wang (1989) to the case of quasicrystals with two substitutions. Firstly, for the IQC with six degrees of freedom, the term $\mathbf{g}\cdot\mathbf{R}$, representing the phase difference caused by the displacement field $\mathbf{R}$ of a defect in a crystal, should be replaced by the inner product in six-dimensional space:

$$\tilde{\mathbf{g}}\cdot\tilde{\mathbf{R}} = \mathbf{g}^{\parallel}\cdot\mathbf{R}^{\parallel} + \mathbf{g}^{\perp}\cdot\mathbf{R}^{\perp}, \tag{1}$$

where $\tilde{\mathbf{g}} = \mathbf{g}^{\parallel} + \mathbf{g}^{\perp}$ and $\tilde{\mathbf{R}} = \mathbf{R}^{\parallel} + \mathbf{R}^{\perp}$, with $\mathbf{g}^{\parallel}$ and $\mathbf{R}^{\parallel}$ being the components in physical space and $\mathbf{g}^{\perp}$ and $\mathbf{R}^{\perp}$ the components in the complementary space of the six-dimensional reciprocal vector $\tilde{\mathbf{g}}$ and displacement vector $\tilde{\mathbf{R}}$, respectively. The parallel component $\mathbf{R}^{\parallel}$ is responsible for the elastic deformation around a defect, as in conventional crystals (phonon strain), while the perpendicular component $\mathbf{R}^{\perp}$ leads to a local rearrangement of the basic tiles (phason strain) [*e.g.* Socolar, Lubensky & Steinhardt (1986)], so the term $\mathbf{g}^{\perp}\cdot\mathbf{R}^{\perp}$ in (1) represents the effect of the phason and $\mathbf{g}^{\parallel}\cdot\mathbf{R}^{\parallel}$ represents the effect of the phonon.

For crystals, the displacement field $\mathbf{R}$ caused by a general perfect dislocation in an infinite isotropic medium is calculated with the formula

$$\mathbf{R} = (1/2\pi)\{\mathbf{b}\varphi + \mathbf{b}_e\sin(2\varphi)/4(1-\nu) + \mathbf{bxu}[(1-2\nu)\ln|r|/2(1-\nu) + \cos 2\varphi/4(1-\nu)]\}, \tag{2}$$

where $\mathbf{b}_e$ is the edge component of the Burgers vector $\mathbf{b}$, $\mathbf{u}$ is the unit vector along the positive direction of the dislocation line and ν is the Poisson ratio of the medium [see *e.g.* Hirsch *et al.* (1965)]. Because the IQC is isotropic in elasticity, neglect of the coupling between phason and phonon gives similar expressions for $\mathbf{R}^{\parallel}$ and $\mathbf{R}^{\perp}$ (Wang & Wang, 1993) and $\tilde{\mathbf{R}} = \mathbf{R}^{\parallel} + \mathbf{R}^{\perp}$ can then be expressed as

$$\tilde{\mathbf{R}} = (1/2\pi)\{\tilde{\mathbf{b}}\varphi + \tilde{\boldsymbol{\eta}}\sin(2\varphi)/4(1-\nu) + \tilde{\boldsymbol{\epsilon}}[(1-2\nu)\ln|r|/2(1-\nu) + \cos(2\varphi)/4(1-\nu)]\}, \tag{3}$$

where $\tilde{\boldsymbol{\eta}}$ and $\tilde{\boldsymbol{\epsilon}}$ are six-dimensional vectors corresponding to $\mathbf{b}_e$ and $\mathbf{bxu}$, respectively, in (2) and their components η_i and ϵ_i ($i = 1,2,\ldots,6$) can be obtained as follows.

By giving the six-dimensional indices b_i and u_i ($i = 1,2,\ldots,6$) of the Burgers vector $\tilde{\mathbf{b}}$ and the dislocation line $\tilde{\mathbf{u}}$, respectively:

$$\tilde{\mathbf{b}} = \sum_{i=1}^{6} b_i\tilde{\mathbf{e}}_i, \tag{4}$$

$$\tilde{\mathbf{u}} = \sum_{i=1}^{6} u_i\tilde{\mathbf{e}}_i, \tag{5}$$

their components in physical space can be easily obtained:

$$\mathbf{b}^{\parallel} = \sum_{i=1}^{6} b_i\mathbf{e}_i^{\parallel}, \tag{6}$$

$$\mathbf{u}^{\parallel} = \sum_{i=1}^{6} u_i\mathbf{e}_i^{\parallel}, \tag{7}$$

where the $\tilde{\mathbf{e}}_i$ are the basis vectors in six-dimensional space and the $\mathbf{e}_i^{\parallel}$ are their components in physical space.

Let

$$BU(i,j) = (b_iu_j - b_ju_i)/[2(1+\tau^2)]^{1/2},$$

where $\tau = (1+5^{1/2})/2$ is the golden ratio. The coefficients ϵ_i in the expression

$$\mathbf{b}^{\parallel}\mathbf{xu}^{\parallel} = \sum_{i=1}^{6} \epsilon_i\mathbf{e}_i^{\parallel} \tag{8}$$

can then be deduced to be

$$\begin{aligned}
\epsilon_1 &= BU(2,3) + BU(3,4) + BU(4,5) + BU(5,6) + BU(6,1),\\
\epsilon_2 &= BU(1,6) + BU(3,1) + BU(3,5) + BU(4,5) + BU(4,6),\\
\epsilon_3 &= BU(1,2) + BU(4,1) + BU(4,6) + BU(5,2) + BU(5,6),\\
\epsilon_4 &= BU(1,3) + BU(5,1) + BU(5,2) + BU(6,2) + BU(6,3),
\end{aligned} \tag{9}$$

$$\epsilon_5 = BU(1,4) + BU(6,1) + BU(6,3) + BU(2,3) + BU(2,4),$$

$$\epsilon_6 = BU(1,5) + BU(2,1) + BU(2,4) + BU(3,4) + BU(3,5).$$

With the relation

$$\mathbf{b}_e^{\parallel} = \mathbf{u}^{\parallel}\mathbf{x}(\mathbf{b}^{\parallel}\mathbf{x}\mathbf{u}^{\parallel}) \tag{10}$$

and the definition

$$UBU(i,j) = (u_i\epsilon_j - u_j\epsilon_i)/[2(1+\tau^2)]^{1/2},$$

the coefficients η_i in the expression

$$\mathbf{b}_e^{\parallel} = \sum_{i=1}^{6} \eta\mathbf{e}_i^{\parallel} \tag{11}$$

can be easily obtained only by replacement of the $BU(i,j)$ in (9) by the corresponding $UBU(i,j)$.

Therefore, the six-dimensional displacement vector $\tilde{\mathbf{R}}$ can be expressed as

$$\tilde{\mathbf{R}} = \sum_{i=1}^{6} R_i\tilde{\mathbf{e}}_i, \tag{12}$$

with

$$R_i = (1/2\pi)\{b_i\varphi + \eta_i\sin(2\varphi)/4(1-\nu) + \epsilon_i[(1-2\nu)\ln|\mathrm{r}|/2(1-\nu) + \cos(2\varphi)/4(1-\nu)]\}. \tag{13}$$

Secondly, the extinction distance ξ_g of the IQC is calculated as

$$1/\xi_g = S(\mathbf{g}^{\parallel})/(\pi VK), \tag{14}$$

where K is the magnitude of the wave vector $\mathbf{k}$ and $S(\mathbf{g}^{\parallel})/V$ is the scattering amplitude per unit volume. According to Elser (1985) and Zhao, Wang, Cheng & Wang (1988), $S(\mathbf{g}^{\parallel})$ is expressed as

$$S(\mathbf{g}^{\parallel}) = \sum_{1\le i<j<k\le 6} S_1(i,j,k)S_2(i,j,k), \tag{15}$$

where the $S_1(i,j,k)$ represent the phase relationships amongst all the rhombohedra constructed by $\{\mathbf{e}_i^{\parallel}, \mathbf{e}_j^{\parallel}, \mathbf{e}_k^{\parallel}\}$ and the $S_2(i,j,k)$ represent the structure factors of these types of rhombohedra. The $S_2(i,j,k)$ values are dependent on the atomic decoration in the rhombohedra and the simple quasilattice model (Elser, 1985) has been used in our calculations.

3. Influences of several parameters on the splitting of HOLZ lines

In this section, the following parameters have been chosen: a quasilattice constant of 0.90 nm, zone axis $\mathbf{z}^{\parallel}\|[-1.1,1.2,3.1]$, anomalous absorption ratio $U_g'/U_g = 0.05$. Unless otherwise stated, the calculations for Figs. 2–5 were conducted for a specimen thickness $t = 100$ nm and a depth of dislocation in the foil de = $t/2$, with $\tilde{\mathbf{b}} = 1/2[0,-1,0,-1,1]$, $\tilde{\mathbf{u}}\|[0,0,0,0,0,1]$ and an accelerating voltage of 100 kV.

In most cases, the transmitted intensity as a function of the deviation angle Δ from the Bragg condition was calculated by using the two-beam dynamical approximation. The degree of splitting of HOLZ lines (induced by a defect) may be described by the following parameters: (*i*) r, the intensity ratio of the split subsidiary peaks (subpeaks) to the major peak; (ii) δ, the angular distance between the subpeak and the major peak, which can be written as $\delta = \Delta_{\text{major}} - \Delta_{\text{sub}}$, where Δ_{sub} and Δ_{major} are the deviation angles of the subpeak and major peak, respectively; (iii) n_s, the number of apparent subpeaks. Generally, the greater the value of r, $|\delta|$ or n_s, the more severe the splitting of the HOLZ line.

Figs. 1(*a*)–(*c*) are references for studying the splitting and shifting behaviours of HOLZ lines, caused by the presence of dislocations. Fig. 1(*a*) shows experimental (left) and simulated (right) $[-1.1,1.2,3.1]$ zone-axis HOLZ-line patterns. For the simulated pattern, the quasilattice constant $a = 0.90$ nm, the accelerating voltage is 200 kV, the anomalous absorption ratio $U_g'/U_g = 0.05$, the thickness of the sample $t = 140$ nm and four beams (*i.e.* $\tilde{\mathbf{g}}_1$, $\tilde{\mathbf{g}}_2$, $\tilde{\mathbf{g}}_3$ and the transmitted beam) are included. The indices n_j ($j = 1,\ldots,6$) of the three reflection vectors $\tilde{\mathbf{g}}_i$ ($i = 1, 2, 3$), their coordinates F_1, F_2 and F_3 in physical space, the inner products $\tilde{\mathbf{g}}\cdot\tilde{\mathbf{b}}$ in six-dimensional space and their corresponding inner products $\mathbf{g}^{\parallel}\cdot\mathbf{b}^{\parallel}$ in physical space are listed in Table 1. Figs. 1(*b*) and (*c*) show intensity profiles of the (2,8,8,−2,−8,−2) HOLZ reflection calculated with foil thicknesses of 100 and 200 nm, respectively, quasilattice constant $a = 0.9$ nm, an accelerating voltage of 100 kV and an anomalous absorption ratio $U_g'/U_g = 0.05$. (In our calculation of intensity profiles, the two-beam approximation is always used.) Obviously, the HOLZ line becomes narrower when the specimen thickness increases.

In the following, we report the calculated results, which show the influences of several parameters on the splitting and shifting behaviour of HOLZ lines induced by dislocations. These parameters are: the distance di between the electron probe and the dislocation core, the depth de at which dislocation lies under the top surface of the sample, the thickness t of the sample and the value of $\tilde{\mathbf{g}}\cdot\tilde{\mathbf{b}}$. The sign of di is chosen to be positive (or negative) when the electron probe is focused on the side of the dislocation in the direction of $\mathbf{u}^{\parallel}\mathbf{u}\mathbf{z}^{\parallel}$ (or $-\mathbf{u}^{\parallel}\mathbf{x}\mathbf{z}^{\parallel}$).

When |di| decreases, *i.e.* the electron probe shifts to the dislocation, the ratio r, angular distance δ and number of the subpeaks n_s generally increase. This fact can be seen from Fig. 2, which shows that r and $|\delta|$ apparently increase when di decreases from 50 to 20 nm.

Table 1. *The indices of* $\tilde{\mathbf{g}}$ *and the values of both* $\tilde{\mathbf{g}}\cdot\tilde{\mathbf{b}}$ *and* $\mathbf{g}^{\parallel}\cdot\mathbf{b}^{\parallel}$ *for three main reflections in Figs.* 1(*a*) *and* 6

HOLZ line no.	n_1*	n_2*	n_3*	n_4*	n_5*	n_6*	F_1	F_2	F_3	$\tilde{\mathbf{g}}\cdot\tilde{\mathbf{b}}$	$\mathbf{g}^{\parallel}\cdot\mathbf{b}^{\parallel}$
1	4	10	2	−6	−4	6	5.09	5.09	0	1	1.17
2	2	2	−6	−4	4	8	5.09	−1.57	2.55	−2	−1.88
3	2	8	8	−2	−8	−2	0	6.67	−2.55	3	3.05

The HOLZ-line splitting behaviour is dependent on the depth de of the dislocation line under the top surface (see Fig. 3). In general, HOLZ lines split most apparently when $de/t \simeq 1/2$ and the splitting behaviour is approximately symmetric about the foil centre. For instance, the intensity profile in the case where the dislocation lies 10 nm below the top surface of the sample is the same as that when the dislocation lies 10 nm above the bottom surface of the sample (de = 90 nm). The same is true for the cases where de = 30 and de = 70 nm (30 nm above the bottom surface).

The splitting behaviour of a HOLZ line varies greatly with changes in the thickness t of the foil specimen. When t increases, the ratio r and number of subpeaks n_s increase, while the angular distance $|\delta|$ decreases (see Fig. 4).

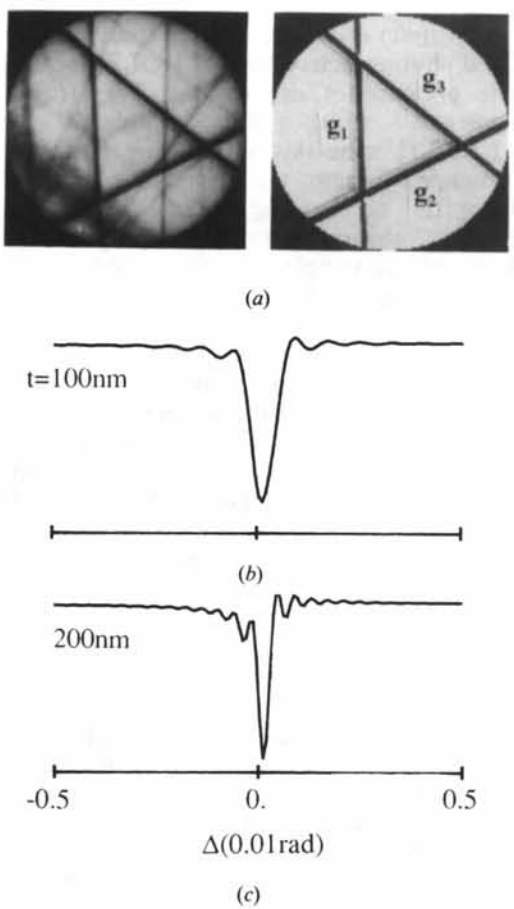

Fig. 1. HOLZ-line patterns and rocking curves of a perfect $Al_{65}Cu_{20}Fe_{15}$ IQC. (*a*) Experimental (left) and simulated (right) [−1.1,1.2,3.1] zone-axis HOLZ-line patterns. For the simulated pattern, the quasilattice constant $a = 0.90$ nm, the accelerating voltage is 200 kV, the anomalous absorption ratio $U_g'/U_g = 0.05$, the thickness of the sample $t = 140$ nm and four beams (*i.e.* $\tilde{\mathbf{g}}_1$, $\tilde{\mathbf{g}}_2$, $\tilde{\mathbf{g}}_3$ and the transmitted beam) are included. (*b*), (*c*) Intensity profiles of the (2,8,8 − 2, − 8, − 2) HOLZ reflection (the two-beam approximation being used) calculated with foil thicknesses of 100 and 200 nm, respectively, quasilattice constant $a = 0.9$ nm, an accelerating voltage of 100 kV and anomalous absorption ratio $U_g'/U_g = 0.05$.

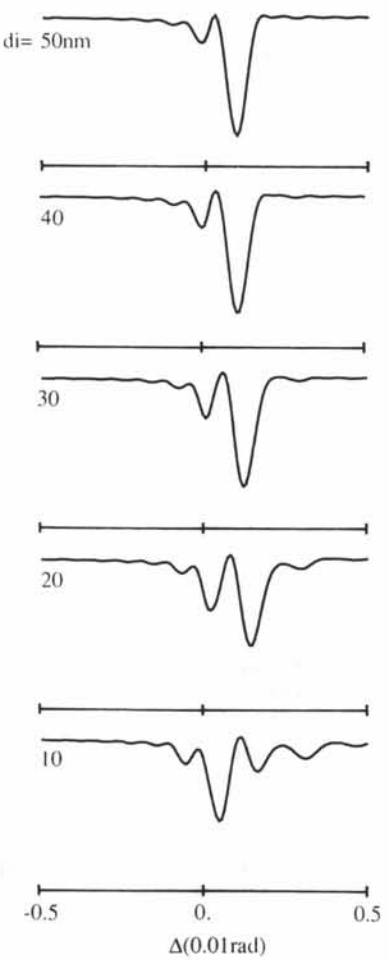

Fig. 2. Changes in intensity profiles of (2,8,8, − 2, − 8, − 2) HOLZ lines with change in distance di. The electron probe is focused on the side of the dislocation pointed to by $\mathbf{u}^{\parallel}\mathbf{xz}^{\parallel}$. The related parameters are $\tilde{\mathbf{b}} = 1/2[0,-1,1,0,-1,1]$, $\tilde{\mathbf{u}} \parallel [0,0,0,0,0,1]$, $t = 100$ nm, de = $t/2$ and $U_g'/U_g = 0.05$.

The value of the inner product $\tilde{\mathbf{g}}\cdot\tilde{\mathbf{b}}$ influences strongly the splitting behaviour of a HOLZ line. The intensity ratio r of the split subsidiary peak to the major peak increases with the value of the inner product $\tilde{\mathbf{g}}\cdot\tilde{\mathbf{b}}$.

Fig. 5 shows the dependence of the sign of δ on the sign of di or $\tilde{\mathbf{b}}$. Reversal of the sign of di [compare Fig. 5(*b*) with Fig. 5(*a*)] or of $\tilde{\mathbf{b}}$ [compare Fig. 5(*c*) with Fig. 5(*a*)] means that the sign of δ is also reversed. The results shown in Fig. 5 may be summarized as

$$\text{sign}(\delta) = -\text{sign}(\tilde{\mathbf{g}}\cdot\tilde{\mathbf{b}}/\text{di}). \qquad (16)$$

However, if the incident probe lies at the dislocation core, the splitting behaviour becomes rather complicated. For example, Fig. 2 shows a reversal of the sign of δ relative to (16) and $n_s = 3$ when di = 10 nm.

4. Simulation of experimental defocus CBED patterns

Based on the above results, we have simulated several experimental CBED patterns from the Al–Cu–Fe IQC. Fig. 6 is an example. Fig. 6(*a*) is an experimental defocus CBED pattern with the dislocation *DD* illuminated. Three main HOLZ lines, $\tilde{\mathbf{g}}_1$, $\tilde{\mathbf{g}}_2$ and $\tilde{\mathbf{g}}_3$, are split into one, two and three nodes, respectively. From the experiment and related analysis, some parameters can be obtained: $\mathbf{u}^{\parallel}\|[1.1,-7.2,3.5]$, $\tilde{\mathbf{b}} = 1/2[0,-1,1,0,-1,1]$, accelerating voltage = 200 kV, zone axis $\|[-1.1,1.2,3.1]$, a = 0.9 nm; the diameter of the defocus area is approximately 120 nm. When the other parameters were chosen to be $U_g'/U_g = 0.05$, foil thickness t = 140 nm, de = $t/2$ and $\tilde{\mathbf{u}}\|[0,2,-4,0,4,-3]$ and three HOLZ reflections $\tilde{\mathbf{g}}_1$, $\tilde{\mathbf{g}}_2$ and $\tilde{\mathbf{g}}_3$ were included, the simulated

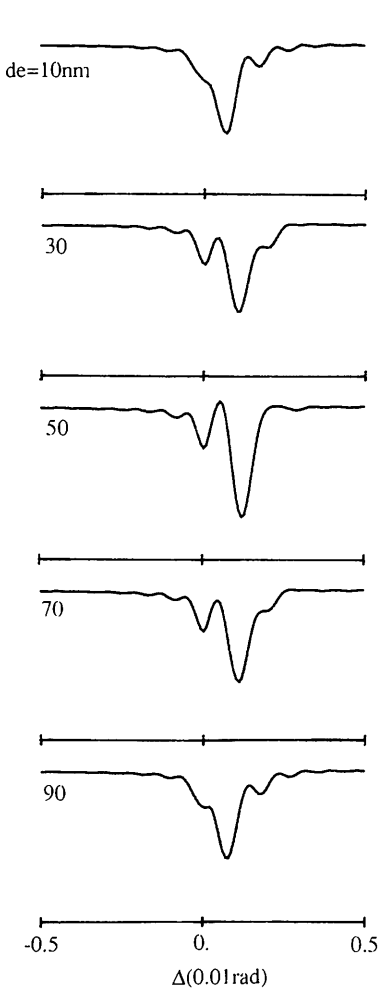

Fig. 3. The influence of the depth de of the dislocation under the top surface on the splitting of HOLZ line (2,8,8,−2,−8,−2). The parameters in this figure are the same as those in Fig. 2 but di = 30 nm is constant and de changes from 10 to 90 nm.

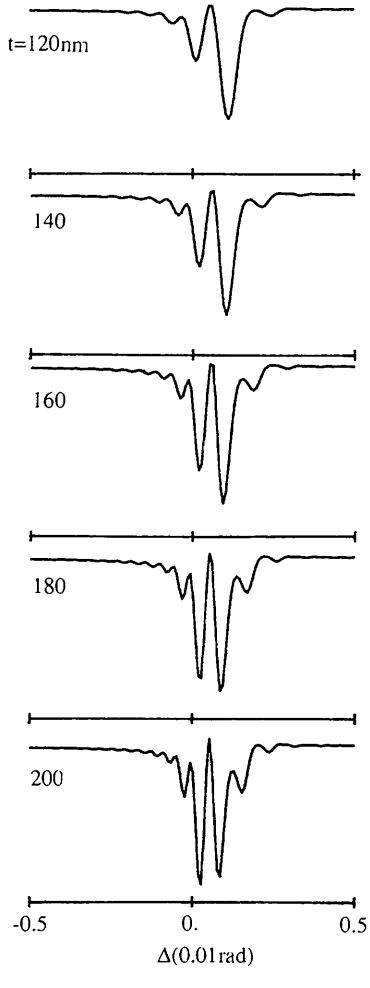

Fig. 4. The influence of the thickness t of the specimen on the splitting of the (2,8,8,−2,−8,−2) HOLZ line. The dislocation is at the middle of the specimen. The other parameters are the same as those in Fig. 2 but di = 30 nm is constant and t changes from 100 to 200 nm.

defocus CBED pattern shown in Fig. 6(*b*) was obtained, in good agreement with the experimental one (Fig.6*a*).

5. Discussion

The good agreement between the experiment and the simulation confirms that the dynamical treatment method of the splitting of HOLZ lines induced by dislocations in the IQC was practicable, although simple assumptions about the displacement field of the dislocation in the IQC and the simple IQC structure model were made.

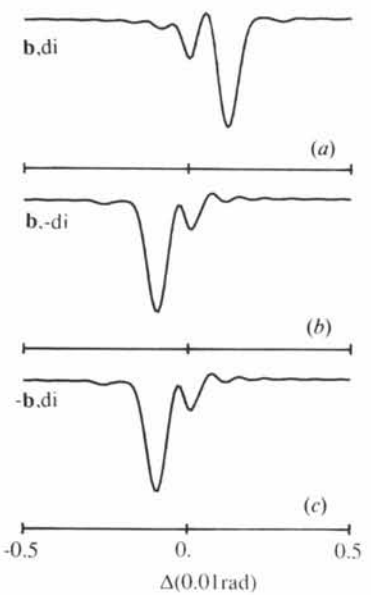

Fig. 5. The influence of the sign of $\tilde{\mathbf{b}}$ or di on the relative positions of the split subpeak. The parameters for (*a*) are $\tilde{\mathbf{b}}$ = 1/2[0, − 1,1,0, − 1,1], $U_g'/U_g = 0.05$, t = 100 nm, de = t/2 and di = 30 nm.

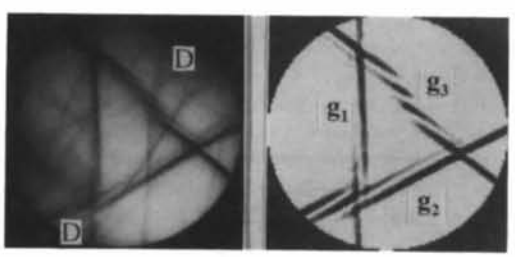

Fig. 6. (*a*) Experimental and (*b*) simulated defocus CBED patterns. For (*b*), three HOLZ reflections $\tilde{\mathbf{g}}_1$, $\tilde{\mathbf{g}}_2$ and $\tilde{\mathbf{g}}_3$ are included, with zone axis $\mathbf{z}^{\parallel} \parallel [-1.1,1.2,3.1]$, accelerating voltage 200 kV, quasilattice constant a = 0.9 nm, foil thickness t = 140 nm, de = t/2, $U_g'/U_g = 0.05$, defocus area of 120 nm in diameter, $\tilde{\mathbf{b}}$ = 1/2[0, − 1,1,0, − 1,1] and $\tilde{\mathbf{u}} \parallel$ [0,2, − 4,0,4, − 3].

The influences of some parameters, such as di, de, t and $\tilde{\mathbf{g}} \cdot \tilde{\mathbf{b}}$, on the splitting behaviours, calculated in this work for an icosahedral quasicrystal, are very similar to those calculated by Zou, Yao & Wang (1991) for a silicon crystal. This is not surprising because the most important difference between the theories for crystals and for quasicrystals lies in the phase factor, which is $\exp(-2\pi i \mathbf{g} \cdot \mathbf{R})$ for crystals and $\exp(-2\pi i \tilde{\mathbf{g}} \cdot \tilde{\mathbf{R}}) = \exp[-2\pi i(\mathbf{g}^{\parallel} \cdot \mathbf{R}^{\parallel} + \mathbf{g}^{\perp} \cdot \mathbf{R}^{\perp})]$ for quasicrystals. As pointed out by Elser (1985), only when $\mathbf{g}^{\perp}$ is small enough can the corresponding reflections $\tilde{\mathbf{g}}$ possess an appreciable intensity. Therefore, we have $\tilde{\mathbf{g}} \cdot \tilde{\mathbf{R}} \simeq \mathbf{g}^{\parallel} \cdot \mathbf{R}^{\parallel}$ and $\tilde{\mathbf{g}} \cdot \tilde{\mathbf{b}} \simeq \mathbf{g}^{\parallel} \cdot \mathbf{b}^{\parallel}$ as revealed in the paper by Wang & Dai (1991) and in Table 1 of this paper; hence, there is no essential difference between the cases of crystals and quasicrystals.

Strictly speaking, the correctness of the perpendicular components $\mathbf{R}^{\perp}$ of the six-dimensional displacement field $\tilde{\mathbf{R}}$ obtained from (3) or (13) by projection is still open to question. However, since the term $\mathbf{g}^{\perp} \cdot \mathbf{R}^{\perp}$ is much smaller than the term $\mathbf{g}^{\parallel} \cdot \mathbf{R}^{\parallel}$, the strict expression for $\mathbf{R}^{\perp}$ is not important for the simulation of the CBED patterns and the contrast images.

References

CHENG, Y. & WANG, R. (1989). *Phys. Status Solidi B*, **152**, 33–37.

ELSER, V. (1985). *Phys. Rev. B*, **32**, 4892–4898.

HEAD, A. K., HUMBLE, P., CLAREBROGH, L. M., MORTOON, A. J. & FORWOOD, C. T. (1973). *Computed Electron Micrographs and Defect Identification*. Amsterdam: North-Holland.

HIRSCH, P., HOWIE, A., NICHOLSON, R. B., PASHLEY, D. W. & WHELAN, M. J. (1965). *Electron Microscopy of Thin Crystals*. Huntington, New York: Robert E. Krieger.

JONES, P. M., RACKHAM, G. M. & STEEDS, J. W. (1977). *Proc. R. Soc. London Ser A*, **354**, 197–222.

KUO, K. H. & WANG, R. (1992). *Electron Microscopy*. Proc. 5th Asia–Pacific Electron Microscopy Conference, pp. 22–27. Singapore: World Scientific.

LU, G., WEN, J., ZHANG, W. & WANG, R. (1990). *Acta Cryst.* A**46**, 103–112.

SOCOLAR, J. E. S., LUBENSKY, T. C. & STEINHARDT, P. J. (1986). *Phys. Rev. B*, **34**, 3345–3360.

TANAKA, M., TERAUCHI, M. & KANEYAMA, T. (1988). *Convergent-Beam Electron Diffraction* II. Tokyo: JEOL Ltd.

WANG, R. & CHENG, Y. (1987). *Mater. Sci. Forum*, **22–24**, 409–420.

WANG, R. & DAI, M. (1993). *Phys. Rev. B*. In the press.

WANG, Z. & WANG, R. (1993). *J. Phys. Condens. Matter*. In the press.

WANG, Z., WANG, R. & DENG, W. (1991). *Phys. Rev. Lett.* **66**, 2124–2127.

ZHAO, D., WANG, R., CHENG, Y. & WANG, Z. (1988). *J. Phys. F*, **18**, 1893–1904.

ZOU, H., YAO, X. & WANG, R. (1991). *Acta Cryst.* A**47**, 490–497.